Engineering Geology 283 (2021) 106026

Contents lists available at ScienceDirect

Engineering Geology

journal homepage: www.elsevier.com/locate/enggeo

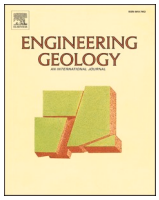

Towards realistic simulations of the impact dynamics of boulders on rock-filled gabion: Combined effects of rock shapes and their crushing strength

Y. Su [a], C.E. Choi [b,*], Y.R. Lv [a], Y. Wang [c], X. Li [a]

[a] College of Mechanics and Materials, Hohai University, Nanjing 210098, China
[b] Department of Civil Engineering, The University of Hong Kong, Pokfulam, Hong Kong Special Administrative Region
[c] College of Water Conservancy and Hydropower Engineering, Hohai University, Nanjing 210098, China

ARTICLE INFO

Keywords:
Rock and boulder fall
Rock-filled gabion
Impact
Crushing
Realistic rock shape
Discrete element method

ABSTRACT

Rock-filled gabions are used to shield barriers and galleries from boulder fall in mountainous regions. A challenge in the design of rock-filled gabions lies in the estimation of the impact and transmitted loads. Furthermore, the effects of irregular rock shapes and rock crushing during the impact process compound the difficulty in estimating the design loads. In this study, a discrete element method model was used to conduct a parametric study to investigate the combined effects rock shape (bulky and flaky) and crushing strength (20 to 50 MPa) on the dynamic response of rock-filled gabions subjected to an impact energy of 70 kJ from a boulder. Results show that rounder rocks should be used to attenuate concentrated impact loading for rocks with a high crushing strength (50 MPa in this study). The maximum impact and transmitted loads on flaky rocks are about 20% larger compared to bulky rocks. The angularity of flaky rocks form force chains that restrict rotation so that they can sustain high loads. In contrast, angular rocks should be used for rocks with low crushing strength (20 MPa in this study). The maximum boulder impact and transmitted loads, respectively, for flaky rocks are about 20% and 33% less than those for bulky rocks. Flaky rocks help to reduce transmitted loads and distribute loading more uniformly. A 30% increase in cushion thickness is recommended to ensure robust cushioning performance for flaky rocks with a crushing strength of 20 MPa.

1. Introduction

Rock-filled gabions are widely used in mountainous regions to reduce the impact loads exerted by rock and boulder fall on protection structures (Lambert et al., 2009, 2014; Green et al., 2018). Field-scale experiments have been conducted to investigate the mechanical response of rock-filled gabions (Lambert, 2007; Lambert and Bourrier, 2013; Ng et al., 2016). Experimental measurements showed that the stress redistribution in the force chains govern the overall mechanical response of the cushioning layer. More interestingly, the shape of the rocks and their crushing strength played a significant role in the complex cushioning response of rock-filled gabions. However, it remains unclear how significant the effects of rock shape and rock crushing strength are to the overall mechanical behaviour of a rock-filled gabion. Evidently, an understanding of the contributions of rock shapes and rock crushing strength at the grain-scale is required to potentially optimise rock-filled gabion cushioning layers.

The discrete element method (DEM) is an ideal tool for studying the mechanical response of rock-filled gabions because the DEM explicitly simulates the formation and collapse of force chains, which ultimately gives rise to an average force exerted on structures under protection (Bertrand et al., 2005; Tordesillas et al., 2014; Breugnot et al., 2015). DEM simulations have been carried out to study the effects of varying the contact friction among particles in a granular assembly and its bulk density on the distribution of force chains (Muthuswamy and Tordesillas, 2006; Bourrier et al., 2008; Zhang et al., 2017; Su et al., 2019; Su et al., 2020). Numerical results showed that straighter force chains with higher contact friction can sustain high loads. Furthermore, force chains comprising smaller particles may collapse more easily. Evidently, a discrete approach is necessary to model grain-scale interactions and to shed light on the complex cushioning mechanisms of rock-filled gabions.

Spheres are most commonly adopted to model granular materials

* Corresponding author.
E-mail address: cechoi@hku.hk (C.E. Choi).

https://doi.org/10.1016/j.enggeo.2021.106026
Received 14 November 2020; Received in revised form 20 January 2021; Accepted 29 January 2021
Available online 31 January 2021

when using the DEM (McDowell and Bolton, 1998; Alaei and Mahboubi, 2012; McDowell and Bono, 2013; Tordesillas et al., 2014; Bone and McDowell, 2015). However, in reality, natural rocks are seldom spherical. Instead they exhibit some degree of angularity. Capturing the effects of angularity is important because it plays an important role in restricting the rotation and rearrangement of particles in granular assemblies (Holubec and D'Appolonia, 1972). Ring shear test were conducted to study the influence of particle shape on the mobilised friction of a granular assembly (Chan and Page, 1997). The experimental results showed that the internal friction angle increases with the particle shape irregularity. Similarly, Ting (1995) used the DEM to examine the effects of rock shape on the mechanical responses of granular materials under biaxial compression. In their DEM simulations, polygonal particles were formed by using bonded round particles to vary particle morphology. It was concluded that the average coordination number, which characterises the number of contacts on each rock, increases with angularity. This further increases the friction angle of the granular assembly. Also, it is interesting to note that Jensen et al. (2001) carried out DEM simulations to model quasi-static two-dimensional ring shear experiments. Their results showed that as particle morphology become more angular, interlocking between grains increased, leading to a greater overall shearing resistance of the granular assembly. Evidently, the aforementioned studies show the importance of capturing particle shape effects, which govern the strength and stiffness of granular assemblies.

Due to a lack of experimental data and the need to simplify the complex grain-scale mechanism of crushing, it is commonly modelled using two approaches in the DEM. One approach is where crushing is governed by the octahedral shear stress, which is based on a Weibull distribution of strength. If the induced shear stress exceeds the particle strength, then a large sphere is replaced with a clump of small spheres with same volume. A quasi-static one-dimensional compression test was modelled using this method (McDowell and Bono, 2013). Their results revealed that by using this approach, the appropriate mechanical response of sand could be obtained. However, the difficulty in adopting this method lies in determining a suitable crushing criterion and crushing pattern. Furthermore, the replacement of large particles with small ones may cause numerical instability because of sudden large contact forces that are generated between particles.

Another method to simulate crushing includes the simulation of rock as an agglomerate of bonded spheres with parallel bonds. Alaei and Mahboubi (2012) simulated quasi-static triaxial loading to study the effects of crushing on the shear resistance of rockfill. Their results showed that at high confining stress, small particles were less prone to crushing. The high crushing strength of small particles increased the interlocking effect among grains and dilatancy. Furthermore, Afshar et al. (2017) simulated quasi-static one-dimensional compression tests on rockfill to investigate the effects of particle shape and crushing on its mechanical response. Three rock shapes, specifically bulky, elongated and flaky were modelled. Bulky rock assemblies were reported to exhibit the highest compression strength and stiffness. In contrast, an assembly of flaky rocks exhibited the lowest compression strength and stiffness. Also, particle crushing was more prominent for flaky assemblies compared to bulky ones. Their findings corroborated that rock crushing is strongly influenced by the rock shape.

Unlike the aforementioned quasi-static loading tests, the dynamic responses of rock-filled gabions in previous field impact tests (Lambert et al., 2014; Ng et al., 2016; Su and Choi, 2020) are highly influenced by the boulder impact energy. At a low boulder impact energy, the dominant cushioning mechanism of a rock-filled gabion may rely on the rock rearrangements, which is governed by the angularity of natural rock shapes. The densification process is significantly influenced by the angularity of natural rock shapes. On the contrary, at a high boulder impact energy, the dominant cushioning mechanism of a rock-filled gabion may rely on crushing, which is governed by the rock crushing strength. However, the combined effects of realistic rock shapes and crushing strengths on the cushioning performances of rock-filled gabions has not yet been elucidated.

In this study, a 3D DEM model with the combined features of realistic rock shapes and rock crushing strength is used to simulate boulder impact on rock-filled gabion cushioning layers. Unconfined compression tests were carried out in the lab on several rock cores to calibrate the parameters required to model crushing in the DEM. Realistic rock morphologies were generated by transferring the digital images to 3D point clouds using photogrammetry. The realistic morphologies were then imported to the DEM model. A parametric study was carried out to examine the combined effects of particle shape and crushing strength on the dynamic response of a rock-filled gabion.

2. Methodology

In this study, Particle Flow Code PFC^{3D} was adopted to simulate a boulder impacting a rock-filled gabion cushioning layer. Clumps are widely adopted to model the effects of particle shape on the mechanical responses of granular materials (Ting, 1995; Su et al., 2020). Clumps composed of assembly of small balls are widely adopted to model the rocks contained in gabion baskets (Golchert et al., 2004; Schubert et al., 2005). The contact law between each particle is governed by a linear parallel bond model. It can be considered as a combination of a linear elastic model and a parallel bond model (Itasca, 1999). The force for a linear elastic model is generated by the compression of springs with constant normal and shear stiffnesses. For each time step, the normal contact force is the product of the incremental overlap and the normal contact stiffness for each particle. The shear contact force for each particle is the product of the incremental overlap and the shear contact stiffness. The shear contact force is governed by Coulomb's law of friction. The equations used to compute the incremental normal dF_n and shear dF_s forces are given as follows (Itasca, 1999):

$$dF_n = k_n d\delta_n \tag{1}$$

$$dF_s = k_s d\delta_s \ (F_s \le \mu F_n) \tag{2}$$

where k_n and k_s are the normal and shear contact stiffness (N/m), respectively, and $d\delta_n$ and $d\delta_s$ are the incremental normal and shear displacements (m), respectively.

The parallel bond model can sustain tension and shear, and resist bending moment until the strength limit is exceeded and the bond breaks. The equations to calculate the parallel bond forces are given as follows:

$$dF_n' = k_n' A d\delta_n \tag{3}$$

$$dF_s' = k_s' A d\delta_s \tag{4}$$

$$A = \pi R^2 \tag{5}$$

where dF_n' and dF_s' are the incremental normal and shear contact forces of parallel bonds (N), respectively, k_n' and k_s' are the normal and shear contact stiffness of parallel bonds (N/m^3), respectively, A is the cross-sectional area of a parallel bond (m^2), R is the minimum radius of two contacting ball (m).

3. Discrete element modelling

3.1. Model calibration

To calibrate the DEM model, 20 cylindrical rock cores (Figs. 1a) with a height of 200 mm and a radius of 50 mm were subjected to unconfined compression following the ASTM Standard D2398-95 (ASTM, 2002). The measured rock density is about 2700 kg/m^3. The measured loading curves for the rock cores were then used to calibrate the DEM model. A cylinder with the same dimensions as the cylindrical rock-cores was simulated using the DEM (Figs. 1b). The adopted particle sizes range

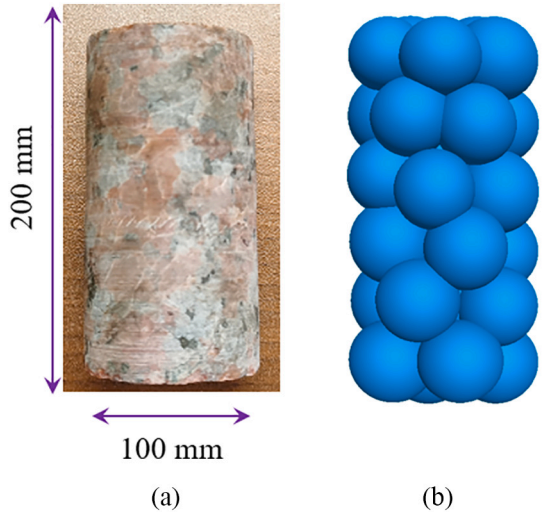

Fig. 1. (a) specimen of rock core in lab test; (b) simulated rock core in PFC3D (particle size: 20 mm–24 mm).

from 20 mm to 24 mm. The calibration parameters include the local friction angle (φ), the normal stiffness (k_n) and the shear stiffness (k_s) of the linear contact between balls, the normal stiffness (pbk_n) and the shear stiffness (pbk_s) of the parallel bond, the minimum tensile strength (pbt_{min}) and maximum tensile strength (pbt_{max}) of the parallel bond.

The measured loading results show that the peak loads range from 22 MPa to 46 MPa. The variability in peak load obtained is attributed to the random internal flaws and discontinuities in the natural rock samples adopted for compression testing (Yang et al., 2007; Turichshev and Hadjigeorgiou, 2017; Afshar et al., 2017). Fig. 2 shows a comparison of the measured stress-strain behaviours between the highest and lowest peak compression loads of 46 MPa and 22 MPa, respectively. For the lowest compression load (i.e., 22 MPa), an obvious drop in stress was caused by asperity crushing at the side of the specimen. This was observed at the axial strain of 0.4%. After the observed stress drop, the stress peaked and then rapidly diminished to zero as the specimen split into two pieces. Similar loading and unloading curves representative of the stress-strain behaviour were also observed for the highest compression loads of 46 MPa. To match the peak compression loads, minimum bond tensile strengths (t_{min}) of 6 MPa and maximum bond tensile strengths (t_{max}) of 12 MPa were selected to describe the rock strength based on the lowest and highest peak stresses measured from the unconfined compression tests. The computed stress peaks and loading and unloading slopes agree well with the measured curves of the unconfined compression tests. The agreement indicates that the calibration parameters are suitable for modelling the quasi-static mechanical response of a rock core. The calibrated parameters are summarized in Table 1.

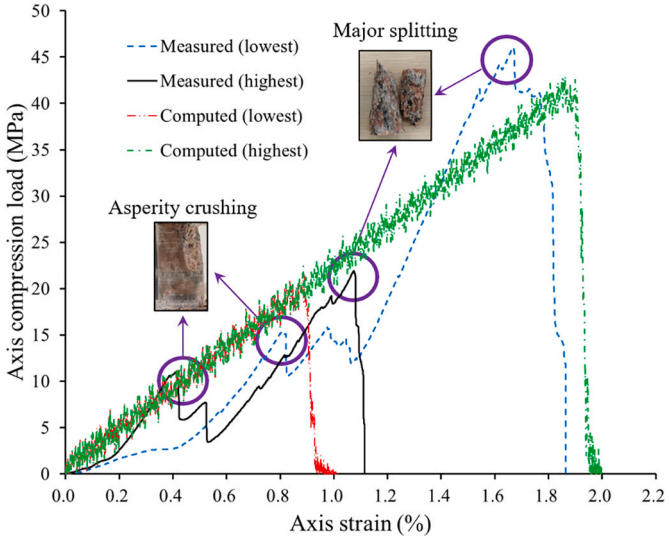

Fig. 2. Comparisons of mechanical responses for rock core between computed and measured results.

3.2. Simulation of realistic particle shape

A total of 40 natural and realistic rock fragment morphologies were replicated in this study. The elongation index ($E_I = d_y/d_x$) and flatness index ($F_I = d_z/d_x$) were used to characterise the morphologies (Janoo, 1998; Jensen et al., 2001; Wang et al., 2015). The length scales d_x, d_y and d_z represent the dimensions of a piece of natural rock along three axes. The d_x and d_z are the longest and shortest dimensions of a natural rock fragment, respectively. The elongation index and flatness index range from 0.3 to 1.0 and 0.3 to 0.8, respectively. The elongation index and flatness index increase as the roundness of the rock increases. This means that if the elongation index and flatness index are unity when the rock is spherical. In contrast, if the elongation index and flatness index are close to zero, then the rock is needle-like.

Two extreme natural and realistic rock shapes, specifically bulky and flaky (Fig. 3a and b), were selected to shed light on the effects of sub-rounded and angular rock shapes on the mechanical responses of rock-filled gabions subjected to dynamic boulder impact. Natural rock shapes are representative of the rock fragments used by Ng et al. (2016). Bulky rocks have an elongation index $E_I = 0.9$ and a flatness index $F_I = 0.8$. Flaky rocks have an elongation index $E_I = 0.3$ and a flatness index $F_I = 0.3$. A summary of rock shapes used in this study is given in Table 2.

To generate realistic 3D renditions of rock morphologies, 48 photos were taken at three different heights around each rock to capture its shape from the side. Then, 10 photos were taken from above each rock to ensure the accuracy of the established rock morphology. Two software, Visual SFM and Meshlab, were used to generate 3D point clouds based on the principle of photogrammetry. The natural rock morphologies were imported to PFC3D (Fu et al., 2017; Afshar et al., 2017). The wall function in PFC3D was then used to stitch together different walls to replicate the bulky and flaky rock shapes (Fig. 4a and b). The scanned natural rocks are much smaller compared to that used in field tests (Ng et al., 2016). To replicate the same dimensions as those in the field test, the three dimensions, d_x, d_y and d_z of the generated clump were increased 4.2 times and 3.2 times for bulky and flaky rocks, respectively, compared to that of the natural rock. The volume of the generated clump is the same as the balls with a particle radius of 0.11 m, which is the average size of rocks typically used in the field to form rock-filled gabions (Ng et al., 2016). Each clump was formed by aggregating overlapped spherical particles with a radius that varies from 20 to 24 mm. Afterwards, parallel bonds were used to join contacting particles. The unit mass for a bulky or flaky rock is about 17 kg. The computed density is about 2930 kg/m^3. The difference between the measured density and

Table 1
DEM Model parameters used in current study.

Parameters	Values
Density (kg/m^3)	2450
Friction coefficient, μ	0.5
Minimum radius, R_{min} (mm)	20
R_{max} / R_{min}	1.2
Normal stiffness, k_n (N/m)	3.0×10^5
Shear stiffness, k_s (N/m)	1.5×10^5
Normal stiffness, k_n' (N/m^3)	4.0×10^{10}
Shear stiffness, k_s' (N/m^3)	2.0×10^{10}
Minimum tensile strength, t_{max} (MPa)	6
Maximum tensile strength, t_{min} (MPa)	12

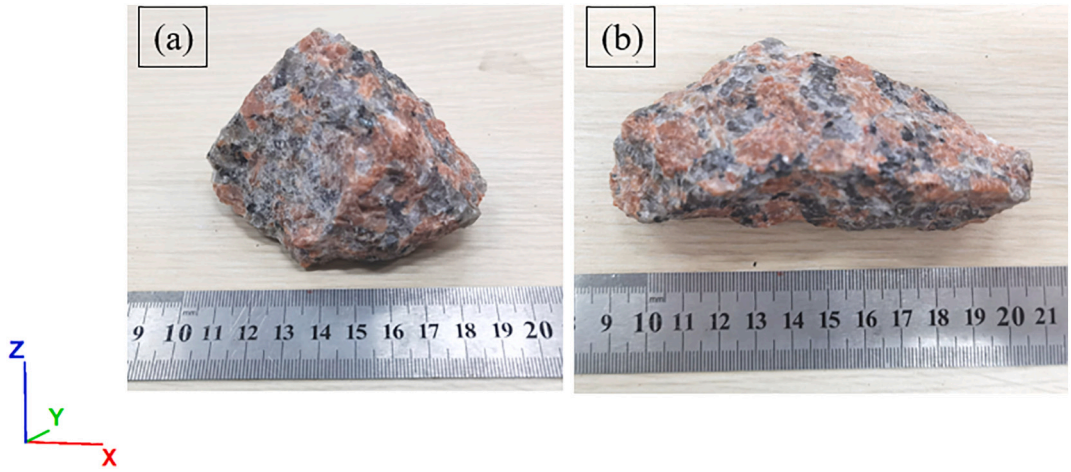

Fig. 3. Natural rock: (a) bulky shape (EI = 1.1, FI = 0.8); (b) flaky shape (EI = 3.1, FI = 0.3).

Table 2
Summary of bulky shape and flaky shape.

Test ID	Rock morphology and generated cluster	d_x (mm)	d_y (mm)	d_z (mm)	Elongation index (E_I)	Flatness index (F_I)
Bulky (B)		66	60	55	0.9	0.8
	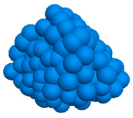	274	249	228		
Flaky (F)		110	35	30	0.3	0.3
	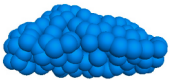	354	113	97		

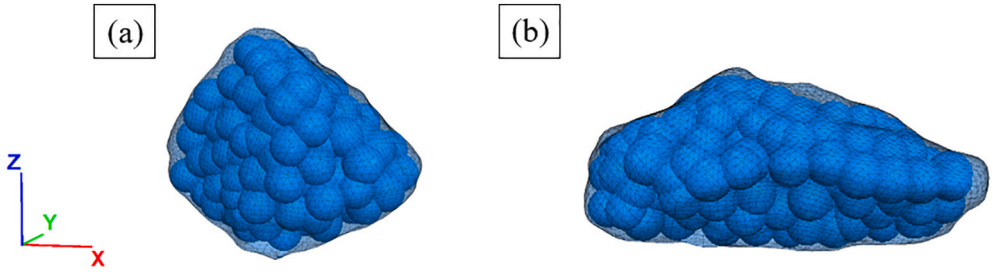

Fig. 4. Simulated rock fragment by sing Bonded-Particle-Method (BPM) in PFC3D: (a) bulky shape; (b) flaky shape.

the computed density is less than 10%.

3.3. Model setup

The clumps with a volume of 0.006 m^3 were generated inside a box to represent the entire gabion cushioning layer. Each cushioning layer is composed of rocks with the same shape. These clumps were allowed to settle in the box under the influence of gravity until the ratio of the average unbalanced force to the average contact force was smaller than 1%. The cushioning layer has a length of 3 m, width of 1 m, and height of 3 m (Fig. 5). The porosities are 0.34 and 0.37 for bulky and flaky rocks, respectively. In previous field tests (Ng et al., 2016), the gabion basket was filled with rock fragments and then the individual baskets were piled up to form the cushioning layer. The rock fragments used to construct rock filled gabions generally range from 160 mm to 300 mm in maximum diameter (GEO, 1993). These fragment sizes fall just short of boulder size as classified by British Standards (BSI, 1999). However, to enhance computational efficiency, a box with a length, height and width of 3 m, 3 m and 1 m, respectively, was used instead of modelling the gabion cells in this study. The box approach has been adopted previously by Bourrier et al. (2011) and Su et al. (2019).

After the gabion cushioning layer was generated, an initial velocity

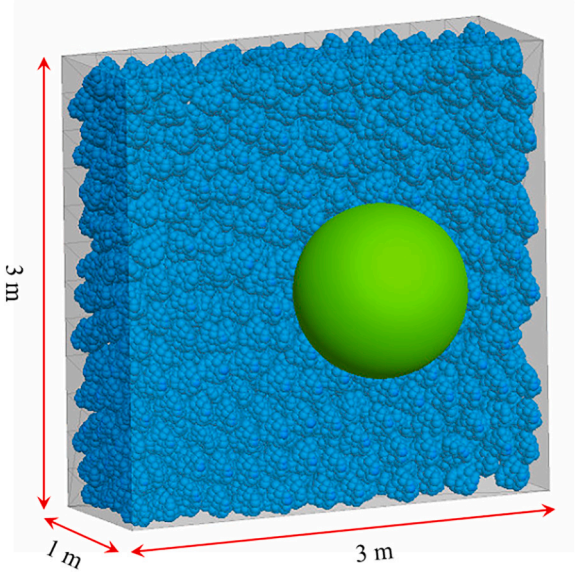

Fig. 5. Oblique view of clusters deposition (bulky shape).

of 8.4 m/s was prescribed to a sphere with a radius of 0.58 m to generate an impact energy of 70 kJ in a similar fashion as that reported in the field tests by Ng et al. (2016). The boulder impact force is recorded during the impact process. To compare the transmitted load distributions on the wall protected by the rock-filled gabion cushioning layer with bulky and flaky rocks, the backside wall is split into 81 individual squares with side lengths of 0.33 m. The transmitted loads on the nine individual walls are recorded during the impact process (Fig. 6).

4. Comparisons between measured and computed results

Fig. 7 shows a comparison of the measured and computed time histories of the boulder impact force (F). Bulky rocks were simulated. As aforementioned, the rock crushing strength from UCS test ranged from 22 MPa to 46 MPa due to the random internal flaws and discontinuities in the natural rock. To study the effect of rock crushing strength, the lowest and highest rock crushing strengths of 20 MPa and 50 MPa were

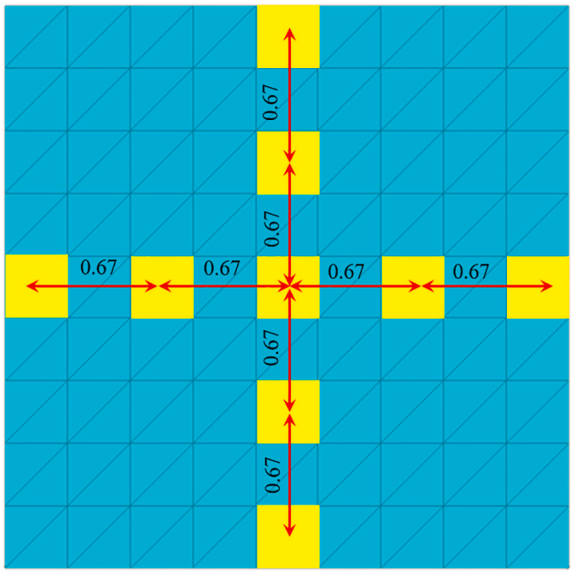

Fig. 6. Nine points of measurements for the computed loads on the rigid barrier (all dimensions in m).

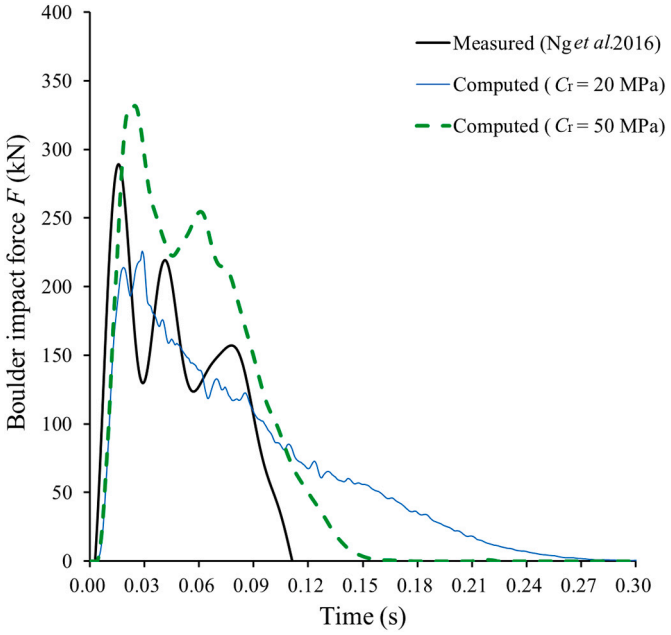

Fig. 7. Comparison of boulder impact forces between measured and computed results (bulky rocks).

adopted to carry out the numerical parametric study. This selected range covers the measured strengths from the UCS tests (i.e., 22 MPa to 46 MPa).

The large fluctuations observed for the measured and computed curves of the boulder impact force may be caused by a rapid lateral displacement of fragments or by the breakage of the fragments during the impact process (Lambert et al., 2009; Su et al., 2019; Su and Choi, 2020). The maximum boulder impact forces of 226 kN and 332 kN were computed for the lowest and highest crushing strengths of 20 MPa and 50 MPa, respectively. This suggests that the boulder impact force increases with rock crushing strength (Lambert et al., 2009). This increasing trend is because force chains composed of rocks with higher crushing strength can sustain high impact loads compared to those with low crushing strength. The computed maximum boulder impact forces for crushing strengths of 20 MPa and 50 MPa are 28% lower and 15% higher, respectively, than the measured maximum boulder impact force of 289 kN reported by Ng et al. (2016). The difference between measured and computed results may be caused by the rock rearrangements, which influence the coordination number and contact point distributions. These influences in turn affect the rock crushing strength and rock crushing pattern. This coincides with the findings reported by Lambert (2007) and Breugnot et al. (2015). Furthermore, the clump is composed of spheres with rather large diameters. This factor may also cause differences in rock shape and contacts, and thus observed difference between the field test (Ng et al., 2016) and the DEM simulation in this study.

5. Effects of rock crushing strength

The crushing strength of the rocks used in the gabions in the field may vary depending on their mineralogy (Taylor and Spears, 1981; Lee and Coop, 1995; Laubscher and Jakubec, 2001; Afshar et al., 2017). To explore the effects of rock crushing strength on the mechanical response of a rock-filled gabion cushioning layer subjected to dynamic boulder impact a parametric study was carried out. The tensile strengths of the parallel bond between particles was adjusted to match the peak compression load (rock crushing strength) measured in the rock core compression tests. Four rock crushing strengths of 20 MPa, 30 MPa, 40 MPa and 50 MPa were tested, corresponding to bond tensile strengths of

5.6 MPa, 8.4 MPa, 11.4 MPa and 14.0 MPa, respectively.

5.1. Boulder impact force and broken bond percentages

Fig. 8a and b show the boulder impact force (F) and the percentage of broken bonds (R_b) for crushing strengths of 20 MPa and 50 MPa, respectively. It has been established in literature that the mechanical response of rock-filled gabion is affected by the combined effects of rock crushing and rock rearrangements or densification (Ng et al., 2016; Su et al., 2019; Lambert et al., 2009; Breugnot et al., 2015). To compare the effects of rock crushing, a dimensionless ratio (R_b) is proposed to characterise the breakage of parallel bonds during impact:

$$R_b = \frac{B_b}{B_t} \tag{6}$$

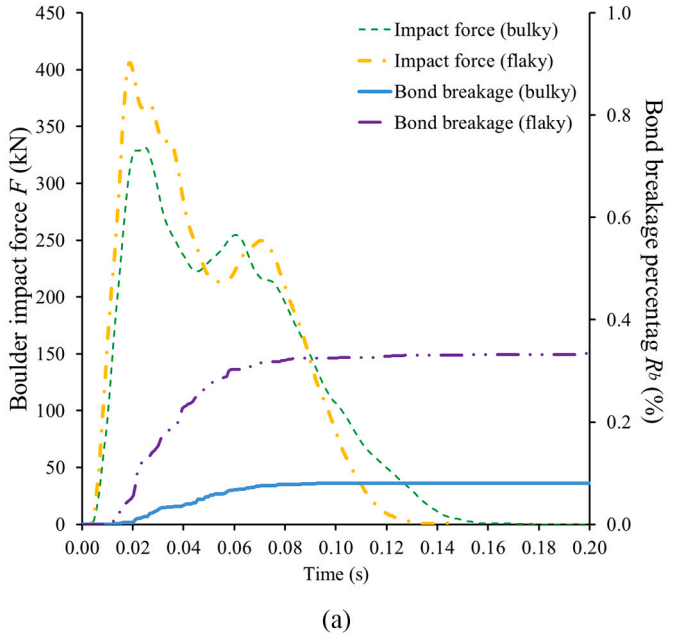

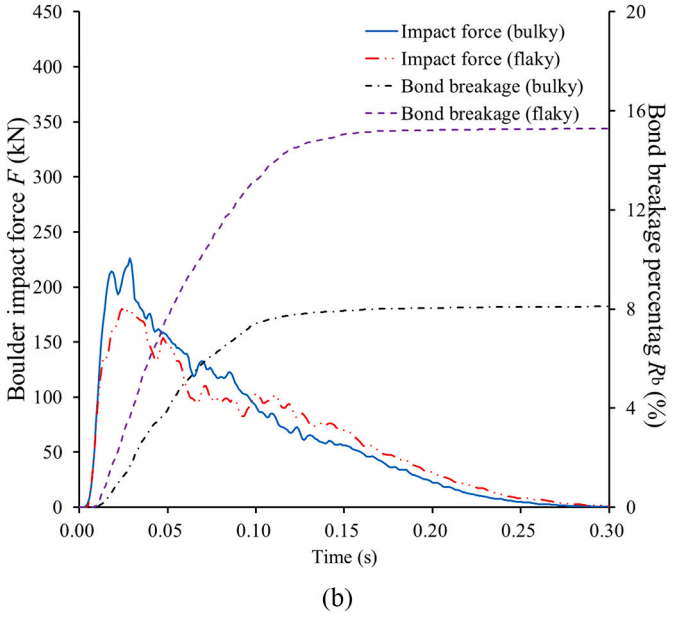

Fig. 8. Time histories of boulder impact force and bonds broken percentage: (a) crushing strength of 50 MPa; (b) crushing strength of 20 MPa.

where B_b represents the number of broken parallel bonds resulting from impact, and B_t represents the total generated parallel bonds number at the beginning of boulder impact.

For a crushing strength of 50 MPa, the percentages of broken bonds are generally less than 0.4% (Figs. 8a). This may imply that that only slight crushing occurred during the impact process, which may still have a strong influence on the granular material impact response. The number of broken clumps is variable depending on the rock shape even for a same ratio of broken bonds. The maximum boulder impact force for flaky rocks is about 22% larger compared to bulky rocks. The high maximum boulder impact force for flaky rocks may be caused by the restricted rotation of the rocks, thereby enabling the force chains to sustain high loads. Fig. 9 shows the effects of rock shape on rotation angle. More specifically, the average rotations of the longitudinal axes of rock fragments during the impact process is examined. The maximum average rock rotation angle for bulky rocks is about 1.4 times larger compared to that for flaky rocks. This confirms that the rock rotations decrease as angularity increases. Similarly, Ting (1995) and Cho et al. (2006) also reported that angularity restricts particle rotation, thereby increasing the strength of a granular assembly.

To further examine the effects of rock shape on the dynamic responses of rock-filled gabions, the average force of rocks contact with boulder are monitored during impact process. Fig. 10 shows that the maximum average contact force for flaky rocks is about 1.6 times larger compared to that for bulky rocks if the rock crushing strength is 50 MPa. This observation may indicate that force chains composed of flaky rocks can sustain higher loads compared to that of bulky rocks. This implies that rounded rocks better attenuate the boulder impact force for fragments with high crushing strength. Furthermore, the loading and unloading slopes for flaky rocks are much steeper compared to that of bulky rocks. The difference in slopes may suggest that angularity enhances the stiffness of a granular assembly.

For the lowest crushing strength simulated (i.e., 20 MPa), the maximum boulder impact force resulting from dynamic impact on the flaky rocks is 20% smaller compared to that of bulky rocks. This means that the resistance of the granular material decreases if the rock shape changes from bulky to flaky. This may be because force chain formed by angular rocks collapse more easily. The collapse of force chains increases the impact duration, thereby reducing the maximum boulder impact force. Meanwhile, the maximum average contact force for flaky rocks is

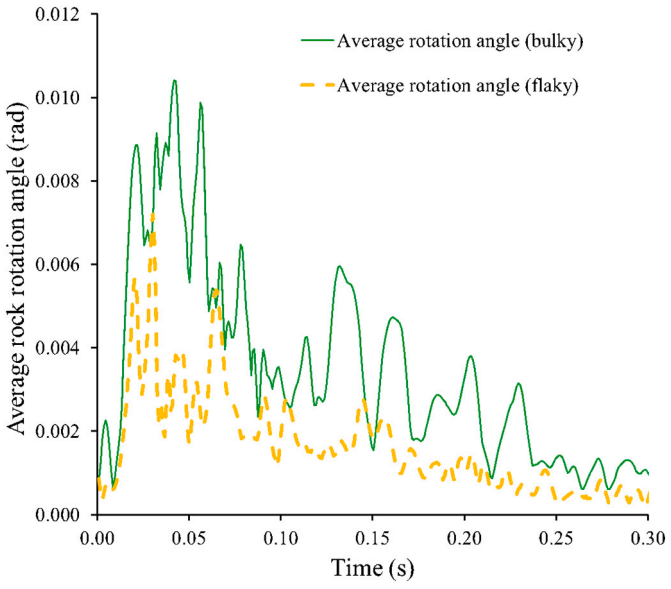

Fig. 9. Comparison of the average rock rotation angle between bulky and flaky rocks.

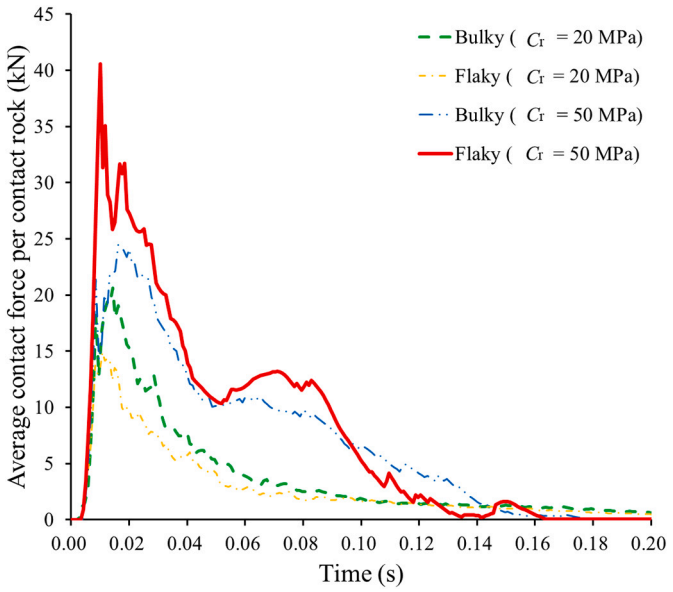

Fig. 10. Comparison of the average contact force per contact rocks between crushing strength of 20 MPa and 50 MPa.

28% smaller compared to that for bulky rocks (Fig. 8). This means that higher loads can be supported by bulky rocks compared to flaky rocks. This trend may be attributed to the fact that rocks that are angular are more susceptible to crushing (Tavares and King, 1998; Golchert et al., 2004; Afshar et al., 2017).

To further examine the effects of rock shape on crushing, the particle-size distributions after impact are computed. The initial particle sizes of 0.22 m are the same for bulky rocks and flaky rocks. Fig. 11 shows a comparison of the particle size distribution curves after boulder impact. If the crushing strength is reduced from 50 MPa to 20 MPa, then the shape of particle size distribution curve changes after impact. This change is because more rocks crush into small particles, which increases the percentage of crushed particles. This observation coincides with the broken bond percentage, which increases as the rock crushing strength decreases (Fig. 8a and b). Furthermore, the particle size distribution curve shifts upwards if the rock shape changes from bulky to flaky shape, implying that flaky rock are more susceptible to crushing. The increased susceptibility is because bulky particles experience contact forces from all directions, while flaky mainly experience forces along the direction of loading. Thus, the deviator stress for flaky rock is larger compared to that for bulky rock. Evidently, the combined effects of rock shape and crushing strength strongly influence the cushioning performance of rock-filled gabions.

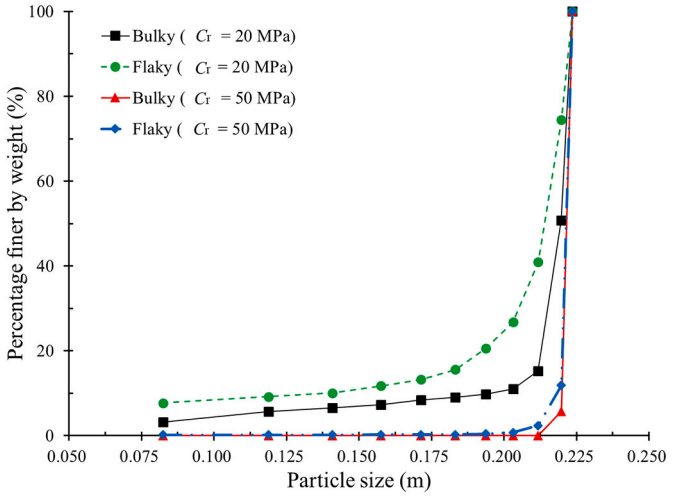

Fig. 11. Comparison of particle-size distribution curve between crushing strength of 20 MPa and 50 MPa.

5.2. *Transmitted loads to the backside wall*

Fig. 12a and b shows comparisons of the computed maximum loads distributions between bulky and flaky rocks. The distributions are computed along the vertical centrelines of the wall. Crushing strengths of 20 MPa and 50 MPa were compared.

At the centre of wall, the maximum transmitted load for flaky rocks is about 1.2 times larger compared to that of bulky rocks for a crushing

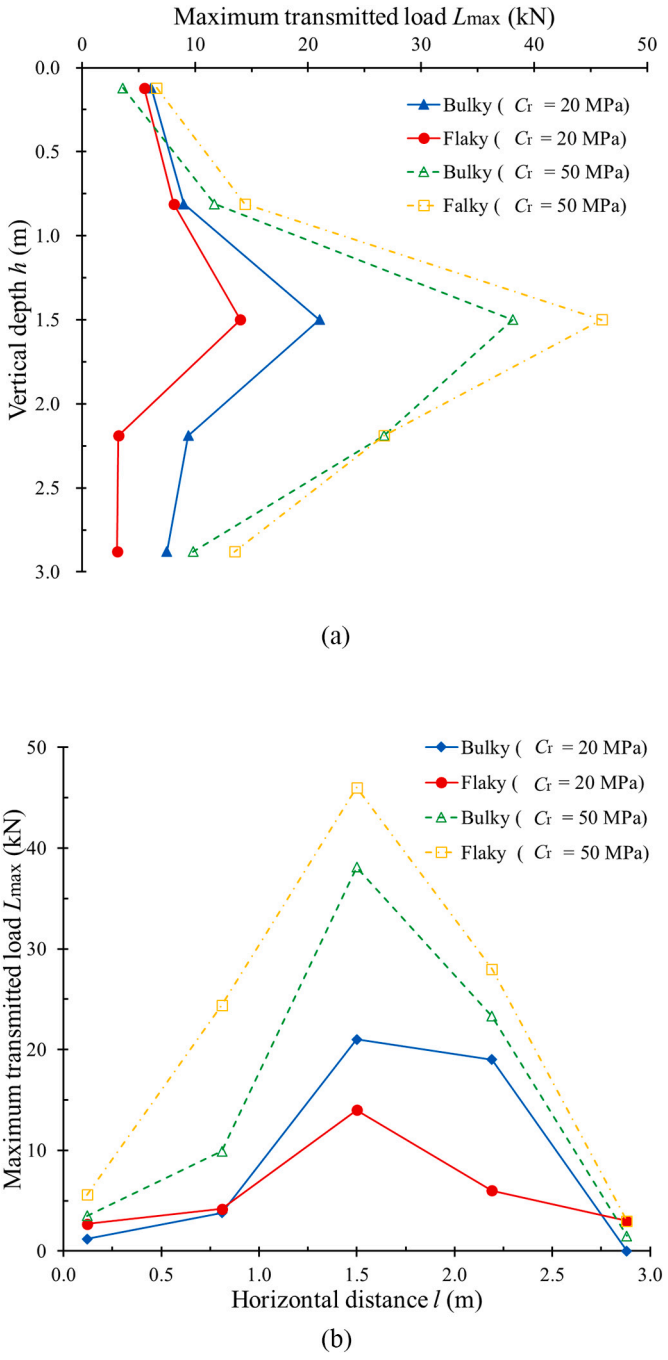

Fig. 12. Comparison of maximum transmitted loads among different particle crushing strengths (σ_c): (a) vertical distributions; (b) horizontal distributions.

strength of 50 MPa. Higher loads are transmitted by granular layers composed of flaky rocks because particle angularity restricts rotation, which strengthens force chains (Fig. 9). If the crushing strength of the rocks is decreased from 50 MPa to 20 MPa, then the maximum transmitted loads to the backside wall decreases by up to 45% and 70% for bulky and flaky rocks, respectively. Furthermore, the maximum transmitted load on flaky rocks is 33% smaller than that on bulky rocks for a crushing strength of 20 MPa. This observation implies that angular rocks can reduce transmitted loads on the backside wall for rocks with low crushing strength because particle crushing strength has been reported to decrease with particle angularity (Tavares and King, 1998; Golchert et al., 2004; Fu et al., 2017). Correspondingly, force chains formed by flaky rocks sustain lower loads compared to those for bulky rocks. (Fig. 10). Thus, lower load transmission occurs with rocks that have low crushing strength and high angularity. The purpose of rock-filled gabions is to reduce loads transmitted on the backside wall. Thus, angular rocks should be used for rocks with low crushing strength.

Fig. 11b shows the computed loads transmitted along the horizontal centreline of the wall. For a crushing strength of 50 MPa, the maximum transmitted loads at the centre wall are about 10.9 and 8.2 times larger compared to those at the horizontal distance of 0.12 m for bulky and flaky rocks, respectively. The transmitted loads decrease with distance from the centre of backside wall. The decrease is attributed to the load mainly being transmitted in the impact direction. It is also reported by the Bourrier et al. (2008) and Zhang et al. (2017) that the force chains carrying the highest loads are generated along the impact direction, and thus transmitted loads are mainly concentrated around the center of the wall. Meanwhile, more energy has been dissipated over longer transmission distances. Longer force chains consist of more particles, which may collapse more easily (Muthuswamy and Tordesillas, 2006). The measured transmitted load at the horizontal distance of 2.2 m is about 2.4 times larger compared to that at the horizontal distance of 0.81 m. This means that the transmitted load is not distributed symmetrically along the horizontal centreline of the wall. The asymmetry is strongly influenced by the stability of formed force chains. Force chains collapse induced by rock rearrangements may cause uneven load distributions on the wall. Moreover, the slope of curves representing the load distributions for flaky rocks at the crushing strength of 50 MPa is steeper compared to that for bulky rocks. This suggests that the transmitted loads are distributed more uniformly by bulky rocks compared to those by flaky rocks.

The slope of the curves represents the load distributions for bulky shaped rocks with a crushing strength of 20 MPa is steeper compared to those for flaky shaped rocks. Therefore, loads are more concentrated at the centre of backside wall for bulky shaped rocks compared to flaky shaped rocks. For the lowest crushing strength of 20 MPa, the transmitted loads are distributed more uniformly with flaky shaped rocks because crushing increases with angularity at low crushing strength (Fig. 11). The crushed rocks fall into the voids between large rocks and further densify the rock-filled gabion. Densification increases contacts and branching points to transfer load over a wider area (Su et al., 2019; Muthuswamy and Tordesillas, 2006).

5.3. Summary of mechanical responses

Fig. 13 shows a comparison of the maximum boulder impact forces and the maximum penetration depths for rock crushing strengths of 20 MPa, 30 MPa, 40 MPa, and 50 MPa. For the highest crushing strength (i.e., 50 MPa), the maximum boulder impact forces resulting from bulky and flaky rocks are 1.5 and 2.3 times, respectively, larger than that of the lowest crushing strength (i.e., 20 MPa). This observation suggests that the maximum boulder impact forces on bulky and flaky shaped rocks decrease with crushing strength. The reduction of the maximum boulder impact force with crushing strength for flaky rocks is 2.1 times higher compared to bulky rocks because flaky rocks with lower crushing strength are more susceptible to crushing compared to bulky rocks

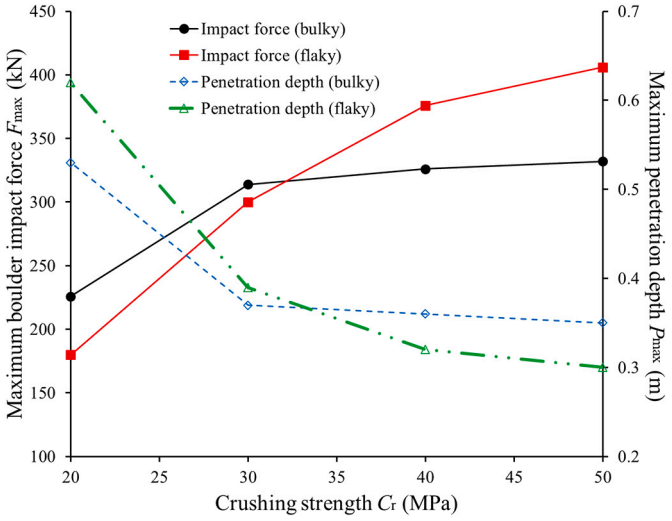

Fig. 13. Comparison of boulder impact forces and penetration depths of rock-filled gabions with different particle crushing strengths (σ_c).

(Fig. 11). Rock crushing prolongs the impact duration, which decreases the maximum boulder impact force.

For high crushing strengths (i.e., 40 MPa and 50 MPa), the maximum boulder impact forces resulting from flaky rocks are about 1.2 times larger compared to the maximum boulder impact force resulting from impact on bulky rocks. Flaky rocks result in a higher maximum boulder impact force because particle angularity restricts rotation and rock rearrangement. Evidently, the combined effects of rock shape and rock crushing strength have a significant influence on the dynamic response of a rock-filled gabion. For a high crushing strength of 50 MPa (highest crushing strength simulated in this study), bulky rocks should be adopted to better attenuate the concentrated boulder impact load. For a low crushing strength of 20 MPa (lowest crushing strength simulated in this study), flaky rocks should be adopted to reduce load transmission.

For a crushing strength of 20 MPa, the maximum penetration depths (P_{max}) in bulky and flaky rocks are 1.5 and 2.1 times, respectively, larger compared to the maximum penetration depth at a crushing strength of 50 MPa. The lower crushing strength results in deeper penetration into the cushioning layer. Excess penetration may compromise a cushioning layer. The minimum thickness of the cushioning layer is recommended as follows (ASTRA, 2008):

$$e \geq P + 3\theta_{max} \tag{7}$$

$$e \geq 2P \tag{8}$$

where e is the required thickness of the cushioning layer (in m); and P is the penetration depth (in m); and θ_{max} is the maximum grain diameter of the cushioning layer (in m). For a rock crushing strength of 20 MPa, the maximum penetration depths for bulky and flaky rocks with a rock crushing strength of 20 MPa are 0.53 m and 0.65 m, respectively. Based on Eqs. (7) and (8), the minimum required thickness are 1.06 m and 1.30 m for bulky and flaky rocks, respectively. Compared to the required minimum thickness, the adopted cushioning thickness of 1 m in this study may not sufficient for flaky rocks with the crushing strength of 20 MPa. For a conservative cushioning layer design, a 30% increase in thickness is recommended to account for lowest crushing strength of 20 MPa.

6. Discussion and conclusions

Rock-filled gabions have proven to be an effective means of reducing the concentrated impact load from large boulders entrained in flow-type landslides. The use of such cushioning layers in an empirical and

prescriptive design manner is somewhat straight forward. However, to specify detailed design requirements, including the size, shape, and density of the rock fragments deserves much more attention.

A calibrated DEM model was used to conduct a parametric study to understand the combined and competing influences of rock shape and rock crushing strength on the performance of a rock-filled gabion cushioning layer subjected to dynamic boulder impact. Capturing the combined effects represents a significant step towards realistic modelling of dynamic impact modelling in the field of geohazard mitigation. Key findings from this study may be drawn as follows:

a) For a rock crushing strength of 50 MPa (highest strength simulated in this study), the maximum boulder impact force and transmitted loads on the flaky rocks are about 20% larger compared to that of bulky rocks. Flaky rocks are angular and restrict rotation, enabling force chains to sustain high loads. This implies that rounded rocks with high rock crushing strength may be more favourable to attenuate loads.
b) For a rock crushing strength of 20 MPa (lowest strength simulated in this study), rocks that are more angular crush more easily. As a result of crushing, the maximum boulder impact force and maximum transmitted loads for flaky rocks are about 20% and 33%, respectively, smaller compared to that for bulky rocks. Thus, flaky rocks should be adopted to reduce load transmission for rocks with low crushing strength.
c) The combined effects of rock shape and rock crushing strength strongly influence the load distributions exerted on structures shielded by a rock-filled gabion cushioning layer. For a crushing strength of 50 MPa, the transmitted loads are distributed more uniformly by bulky rocks compared to flaky rocks. Force chains composed of bulky rocks collapse more easily compared to those composed of flaky rocks. However, for a rock crushing strength of 20 MPa, transmitted loads are distributed more uniformly by flaky rocks compared to those of bulky rocks because flaky rocks crush more easily. Crushed rocks fall into the voids between larger rocks. This process densifies the granular assembly and enhances load transfer through more branching points in the force chains. To help distribute loads onto protection structures more uniformly, flaky rocks are more favourable compared to bulky rocks.
d) The required cushioning layer thickness increases as the crushing strength of the rocks decreases. For a conservative cushioning design, a 30% increase in thickness is recommended to account for flaky rocks with a low crushing strength (i.e. 20 MPa).

Although the work presented in this study represents a step towards realistic simulations of boulders impacting rock-filled gabions, much more work is needed to rationalise existing design guidelines. For instance, the orientation of the rock fragments, variability in the fragments, their bulk density, and the steel-wire gabion cell all influence the dynamic response of the rock-filled gabion, however these variables have yet to be investigated.

The research presented here shows that crushing and realistic shapes do play a significant role in the cushioning response. This is consistent with the qualitative trends reported in the field. However, comparing the computed results from this study directly to field measurements presents difficulties due to the variability of the rock fragments adopted in the field and a lack of detailed account of the preparation of the field rock-filled gabions. Despite the challenges in evaluating the results, the conclusions pertaining to adopting specific rock shapes, such as rounder ones for a more distributed loading response and flaky rocks for lower load transmission, nonetheless are clear advancements in the existing field of research. Furthermore, to generalise the results from this study, the consideration of the variability of crushing strength and inherent flaws of rocks may need to be accounted for. The simulations certainly did not account for abrasion, asperity breakage and major splitting, which are breakage mechanisms that are governed by the shape of the rock and mineralogy. Therefore, the findings from this study support that this is an important and promising fundamental research area that warrants further detailed consideration to enhance geohazard mitigation in mountainous regions around the globe.

Declaration of Competing Interest

The authors declared that they have no conflicts of interest to this work.

We declare that we do not have any commercial or associative interest that represents a conflict of interest in connection with the work submitted.

Acknowledgements

The authors would like to gratefully acknowledge the support from the Natural Science Foundation of Jiangsu Province (Grants No BK20200528), Fundamental Research Funds for the Central Universities (B210202103). The authors are grateful for the financial support from the National Natural Science Foundation of China (51709052). The authors are grateful for the financial support from the National Natural Science Foundation of China (51779264). The authors are also grateful for financial support from the Research Grants Council of the Government of Hong Kong SAR, China (16209717; 16212618; 16210219; 27205320; AoE/E-603/18; T22-603/15N).

References

Afshar, T., Disfani, M., Arulrajah, A., Narsilio, G., Emam, S., 2017. Impact of particle shape on breakage of recycled construction and demolition aggregates. Powder Technol. 308, 1–12.
Alaei, E., Mahboubi, A., 2012. A discrete model for simulating shear strength and deformation behaviour of rockfill material, considering the particle breakage phenomenon. Granul. Matter 14 (6), 707–717.
ASTM, 2002. Standard Test Method for Unconfined Compressive Strength of Intact Rock Core Specimen. ASTM D2398-95. ASTM, West Conshohocken, PA.
ASTRA, 2008. Effects of Rockfall on Protection Galleries. Federal Roads Office, Swiss.
Bertrand, D., Nicot, F., Gotteland, P., Lambert, S., 2005. Modelling a geo-composite cell using discrete analysis. Comput. Geotech. 32 (8), 564–577.
Bone, J.P., McDowell, G.R., 2015. An insight into the yielding and normal compression of sand with irregularly-shaped particles using DEM. Powder Technol. 22 (3), 270–277.
Bourrier, F., Nicot, F., Darve, F., 2008. Physical processes within a 2D granular layer during an impact. Granular Matte 10, 415–437.
Bourrier, F., Lambert, S., Heymann, A., Gotteland, P., Nicot, F., 2011. How multi-scale approaches can benefit the design of cellular rockfall protection structures. Can. Geotech. J. 48 (12), 1803–1816.
Breugnot, A., Lambert, S., Villard, P., Gotteland, P., 2015. A discrete/continuous coupled approach for modelling impacts on cellular geostructures. Rock Mech. Rock Eng. 49 (5), 1831–1848.
BSI, 1999. Code of Practice for Site Investigations. British Standards Institution, London.
Chan, L.C.Y., Page, N.W., 1997. Particle fractal and load effects on internal friction in powders. Powder Technol. 90, 259–266.
Cho, G.C., Dodds, J., Santamarina, J.C., 2006. Particle shape effects on packing density, stiffness, and strength: natural and crushed sands. J. Geotech. Geoenviron. 132 (5), 591–602.
Fu, R., Hu, X., Zhou, B., 2017. Discrete element modelling of crushable sands considering realistic particle shape effect. Comput. Geotech. 91, 179–191.
Geotechnical Engineering Office, 1993. Guide to Retaining Wall Design (Geoguide 1). Geotechnical Engineering Office, HKSAR.
Golchert, D., Moreno, R., Ghadiri, M., Litster, J., 2004. Effect of granule morphology on breakage behaviour during compression. Powder Technol. 143-144, 84–96.
Green, R., Lambert, C., Watts, C., Kennett, D., Ryder, E., 2018. Development and Testing of a Modular Rockfall Protection Wall to Mitigate Earthquake-induced Slope Hazards. 69th Highway Geology Symposium. September 2018.
Holubec, I., D'Appolonia, E., 1972. Effect of particle shape on the engineering properties of granular soils. ASTM Spec. Tech. Publ. 304–318.
Itasca, 1999. PFC 3D-user Manual. Itasca Consulting Group, Minneapolis, Minn.
Janoo, V.C., 1998. Quantification of Shape, Angularity, and Surface Texture of Base Course Materials, Special Report 98–1. Cold Regions Research and Engineering Laboratory, US Army Corps of Engineers.
Jensen, R.P., Edil, T.B., Plesha, M.E., Kahla, N.B., 2001. Effect of Particle Shape on Interface Behavior of DEM-Simulated Granular Materials. Int. J. Geomech. 1 (1), 1–19.
Lambert, S., 2007. Comportement mécanique de géocellules - application aux constituants de merlons pare-blocs cellulaires. PhD thesis. Université Joseph Fourier, Grenoble, France.

Lambert, S., Bourrier, F., 2013. Design of rockfall protection embankments: a review. Eng. Geol. 154, 77–88.
Lambert, S., Gotteland, P., Nicot, F., 2009. Experimental study of the impact response of geocells as components of rockfall protection embankments. Nat. Hazards Earth Syst. Sci. 9 (2), 459–467.
Lambert, S., Heymann, A., Gotteland, P., Nicot, F., 2014. Real-scale investigation of the kinematic responses of a rockfall protection embankment. Nat. Hazards Earth Syst. Sci. 14 (5), 1269–1281.
Laubscher, D.H., Jakubec, J., 2001. The MRMR rock mass classification for jointed rock masses. In: Hustrulid, W.A., Bullock, R.L. (Eds.), Underground Mining Methods: Engineering Fundamentals and International Case Studies. SME, pp. 475–481.
Lee, I.K., Coop, M.R., 1995. The intrinsic behaviour of a decomposed granite soil. Géotechnique 45 (1), 117–130.
McDowell, G., Bolton, M.D., 1998. On the micro mechanics of crushable aggregates. Géotechnique 48 (5), 667–679.
McDowell, G.R., Bono, J.P., 2013. On the micro mechanics of one-dimensional normal compression. Géotechnique 63 (11), 895–908.
Muthuswamy, M., Tordesillas, A., 2006. How do interparticle contact friction, packing density and degree of polydispersity affect force propagation in particulate assemblies? J. Stat. Mech. 2006, P09003.
Ng, C.W.W., Choi, C.E., Su, A.Y., Kwan, J.S.H., Lam, C., 2016. Large-scale successive impacts on a backside wallshielded by gabions. Can. Geotech. J. 53 (10), 1688–1699.
Schubert, W., Khanal, M., Tomas, J., 2005. Impact crushing of particle–particle compounds—experiment and simulation. Int. J. Miner. Process. 75 (1), 41–52.
Su, Y., Choi, C.E., 2020. Effects of particle shape on the cushioning mechanics of rock-filled gabions. Acta Geotech. https://doi.org/10.1007/s11440-020-01080-x (online).
Su, Y., Cui, Y., Ng, C.W.W., Choi, C.E., Kwan, J.S.H., 2019. Effects of particle size and cushion thickness on the impact performance of gabions. Can. Geotech. J. 56 (2), 198–207.
Su, Y., Choi, C.E., Ng, C.W.W., Lam, H.W.K., Wong, L.A. Lee. C., 2020. New light-weight concrete foam to absorb debris-flow-entrained boulder impact: Large-scale pendulum modelling. Eng. Geol. 275, 10724.
Tavares, L., King, R., 1998. Single-particle fracture under impact loading. Int. J. Miner. Process. 54 (1), 1–2854.
Taylor, R.K., Spears, D.A., 1981. Laboratory investigation of mudrocks. Q. J. Eng. Geol. Lond. 14, 291–309.
Ting, J., 1995. Effect of particle shape on the strength and deformation mechanism of ellipse shape granular assemblies. Eng. Comput. 12 (2), 99–108.
Tordesillas, A., Steer, C.A.H., Walker, D.M., 2014. Force chain and contact cycle evolution in a dense granular material under shallow penetration. Nonlin. Processes Geophys 21 (2), 505–519.
Turichshev, A., Hadjigeorgiou, J., 2017. Quantifying the effects of vein mineralogy, thickness, and orientation on the strength of intact veined rock. Eng. Geol. 226, 199–207.
Wang, Y., Dan, W., Xu, Y., Xi, Y., 2015. Fractal and morphological characteristic of single marble particle crushing in uniaxial compression test. Adv. Mater. Sci. Eng. 2015 (1), 1–10.
Yang, J., Zeng, Y., W., and Wu, A, Q., 2007. The uniaxial compressive strength of porphyritic granite. China Rural Water Hydropower J. 2007 (8), 70–75.
Zhang, L., Lambert, S., Nicot, F., 2017. Discrete dynamic modelling of the mechanical behaviour of a granular soil. Int. J. Impact Eng. 103, 76–89.